Journal of *Marine Science and Engineering*

MDPI

*Article*

# Hydrodynamic Performance of High-Speed Craft: A CFD Study on Spray Rails

**Muhammad Sulman [1], Simone Mancini [2,*], Rasul Niazmand Bilandi [3] and Luigi Vitiello [2]**

[1] Department of Naval Architecture, National University of Science and Technology (NUST), PNEC PNS Jauhar, Karsaz Faisal Cantonment, Karachi 75350, Pakistan; muhammadsulman7432@gmail.com
[2] Department of Industrial Engineering, University of Napoli "Federico II", 80125 Napoli, Italy; luigi.vitiello@unina.it
[3] Estonian Maritime Academy, Tallinn University of Technology, 11712 Tallinn, Estonia; rasul.niazmand@taltech.ee
* Correspondence: simone.mancini@unina.it

**Abstract:** In high-speed crafts, whisker spray increases viscous resistance by enlarging the wetted surface near the stagnation line. Spray rails (SRs) mitigate this issue by redirecting water flow, reducing the wetted surface, and lowering overall resistance. This study investigates the effect of SRs on the hydrodynamic performance of the C1 hull of Naples Systematic Series (NSS), focusing on the systematic variations in size, number, and placement. Numerical simulations, validated with towing tank results, were conducted using STAR CCM+ 2306. Mesh independence analysis was also performed to optimize computational efficiency. Key findings highlight the critical role of SR design in performance optimization. Wider SRs (e.g., three per side, 0.96% *LWL*) reduced resistance by up to 8.5% at high speeds ($Fr_{\nabla} = 3.26$), but slightly increased the resistance at lower speeds (~2%) due to a larger wetted surface. Narrower SRs (e.g., three per side, 0.48% *LWL*) achieved resistance reductions of up to 4.6%, while configurations with multiple SRs (e.g., three per side, 0.72% *LWL*) outperformed single-rail designs by reducing resistance up to 4%. Placement near the chine proved more effective than near the keel, offering a 4% additional reduction in resistance. Additionally, SRs generated lift, raising the hull, and reducing immersion. The study underscores the importance of optimizing SR size, number, and placement to enhance hydrodynamic efficiency, particularly for high-speed operations.

**Keywords:** planing boat; spray rails; resistance; hydrodynamic performance; whisker spray reduction; CFD modeling



Academic Editor: Decheng Wan

Received: 8 February 2025
Revised: 21 February 2025
Accepted: 22 February 2025
Published: 25 February 2025

**Citation:** Sulman, M.; Mancini, S.; Niazmand Bilandi, R.; Vitiello, L. Hydrodynamic Performance of High-Speed Craft: A CFD Study on Spray Rails. *J. Mar. Sci. Eng.* **2025**, *13*, 438. https://doi.org/10.3390/jmse13030438



## 1. Introduction

The hydrodynamic performance of high-speed craft (HSC) is a critical determinant of their operational efficiency, safety, and economic viability [1]. Enhancing hydrodynamic performance can be achieved through innovative hull designs or retrofitting features such as steps, tunnels, interceptors, and spray rails [2]. Among these, spray rails play a prominent role in reducing hydrodynamic resistance, improving stability. By deflecting water away from the hull's surface, spray rails minimize the wetted surface area and, consequently, the overall drag. Their effectiveness, however, depends on their shape, quantity, and positioning, necessitating computational tools for performance prediction and optimization.

Planing hulls, operating at high speeds on the water surface, generate significant spray due to the interaction of the hull's wetted surface with the water. This spray contributes

to the total hydrodynamic drag, as documented in foundational studies by Savitsky and Breslin [3], Latorre [4], Savitsky et al. [5], and Savitsky and Morabito [6]. The Savitsky Method [7] has been instrumental in predicting trim and drag based on hull geometry and speed. Although the original method did not quantify spray resistance, subsequent refinements have incorporated whisker spray, which accounts for up to 20% of total resistance at high speeds [5,8]. This underscores the need to quantify and minimize spray resistance for improved fuel efficiency and hydrodynamic performance, aligning with sustainable maritime practices.

For instance, spray rails, particularly when sharp-edged and properly placed, significantly disrupt water flow to minimize resistance. Studies by Clement [9], Savitsky [10], and more recently Seo et al. [11] and Lakatoš et al. [12] highlight the role of spray rails in reducing resistance, improving seakeeping, and enhancing overall stability. Similarly, stepped hulls effectively reduce wetted surface area and enhance lift-to-drag ratios, as demonstrated by Savitsky et al. [13], Garland [14], Taunton et al. [15], and Vitiello et al. [16]. Spray deflectors, though less common, offer another effective solution, with studies reporting drag reductions of 10–20% under optimal configurations [17–19].

Developed mathematical models such as Savitsky [7], Martin [20], Zarnick [21], Van Deyzen [22] and Niazmand Bilandi et al. [23–25] serve as efficient tools for preliminary hull design by predicting resistance, trim, and stability. However, their reliance on empirical correlations limits their application in complex scenarios. In contrast, CFD using the Volume of Fluid (VOF) method offers enhanced capabilities for analyzing complex parameters such as pressure distribution, wetted surface area, and spray-induced resistance. Despite its advantages, CFD faces challenges in accurately modeling planing hulls, often underestimating resistance by 10–20% compared to the experimental data [26,27]. High-fidelity simulations are crucial for optimizing designs and achieving superior performance.

According to the reviewed literature, the effect of different spray rail configurations—sizes, quantities, and positions—on the performance of planing hulls remains unclear and requires further investigation.

This paper presents a comprehensive study into the effects of spray rails on planing hulls, focusing on their influence on whisker spray behavior and total resistance in calm water. Using advanced CFD simulations, the study examined different configurations such as sizes, quantities, and positions on the C1 hull [28], providing valuable insights for design guidelines. The analysis compares hull performance with and without spray rails at three volumetric Froude numbers: $Fr_{\nabla}$ = 1.42, 2.79, and 3.26. The simulations, conducted with CFD software Siemens PLM Star-CCM + 2306 [29], incorporate an overset grid technique and dynamic fluid body interaction (DFBI) for the precise modeling of multiphase dynamics. Validation and mesh independence studies confirm the reliability of the methodology, with results closely aligning with experimental benchmarks.

This work is structured as follows:

- Section 2 outlines the problem definition, along with the base hull and spray rail configurations.
- Section 3 details the numerical equations, boundary conditions, and simulation parameters.
- Section 4 focuses on validation and verification, including mesh independence studies.
- Section 5 presents the results and discussion, emphasizing performance metrics across various configurations.
- Section 6 concludes with key findings and contributions.
- Appendices A and B provide supplementary details, including Y+ contours and tabulated results.

By combining CFD analysis with a systematic approach, this study establishes an outline for improving spray rail designs. The findings contribute to advancing planing hull technology, supporting the development of more efficient and sustainable high-speed craft.

## 2. Problem Definition

When a planing hull operates in planing mode, the bottom of the hull generates two distinct regions: one associated with a high-pressure zone and the other with a spray area, often referred to as the whisker spray area. These regions, depicted in Figure 1, play a crucial role in the hydrodynamic behavior of the craft. As speed increases, the spray area expands, which in turn contributes to the overall resistance experienced by the vessel.

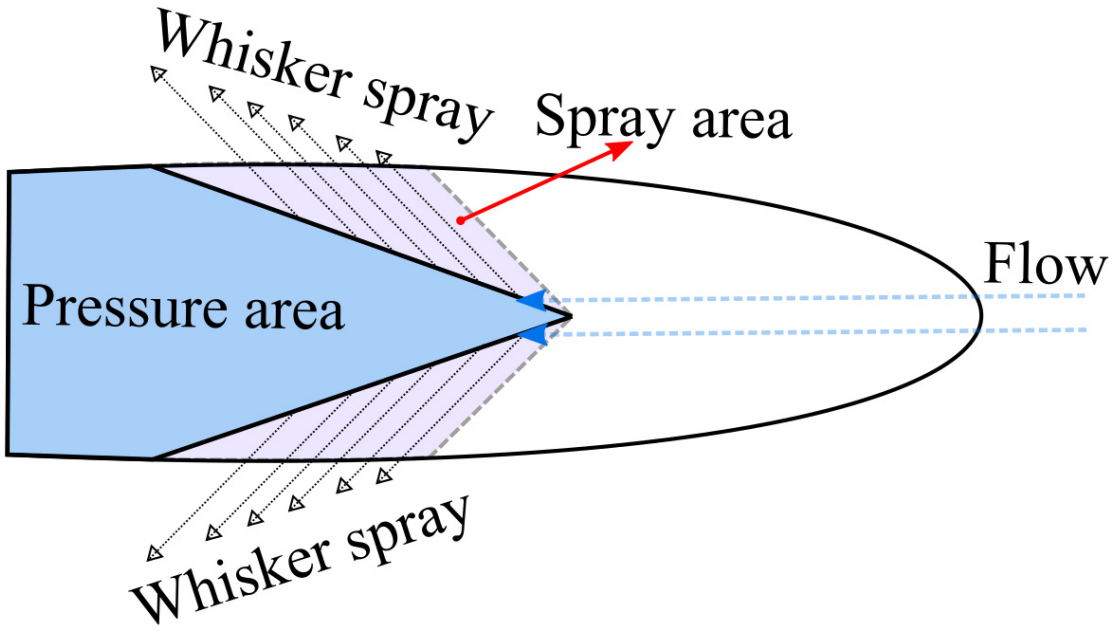


**Figure 1.** Illustration of the pressure and whisker spray regions generated by a prismatic model planing hull, adapted from Savitsky et al. [5].

The whisker spray consists of a mixture of air and water, making it difficult to account for experimental methods that rely on recording wetted surface images for calculations. Although this spray is typically excluded from the wetted surface area during post-processing, it significantly affects the total resistance of the hull. Therefore, managing the whisker spray is essential for improving performance.

To minimize whisker spray, it is important to guide the spray flow toward the transom, which can be effectively achieved using spray rails (Figure 2). Spray rails are primarily designed to control and reduce the impact of water spray emanating from the hull, ultimately enhancing the vessel's performance, efficiency, and onboard comfort. These rails are usually triangular shaped, though their design and placement can vary. The number, location, and alignment of spray rails along the hull remain topics of debate within the maritime industry, as there is no consensus on optimal configuration.

In this study, we aim to investigate the effects of spray rail dimensions, the number of rails, and their positioning on the performance of planing hulls at different speeds. By analyzing these factors using CFD, we hope to provide insights that will improve hull efficiency and reduce overall resistance.

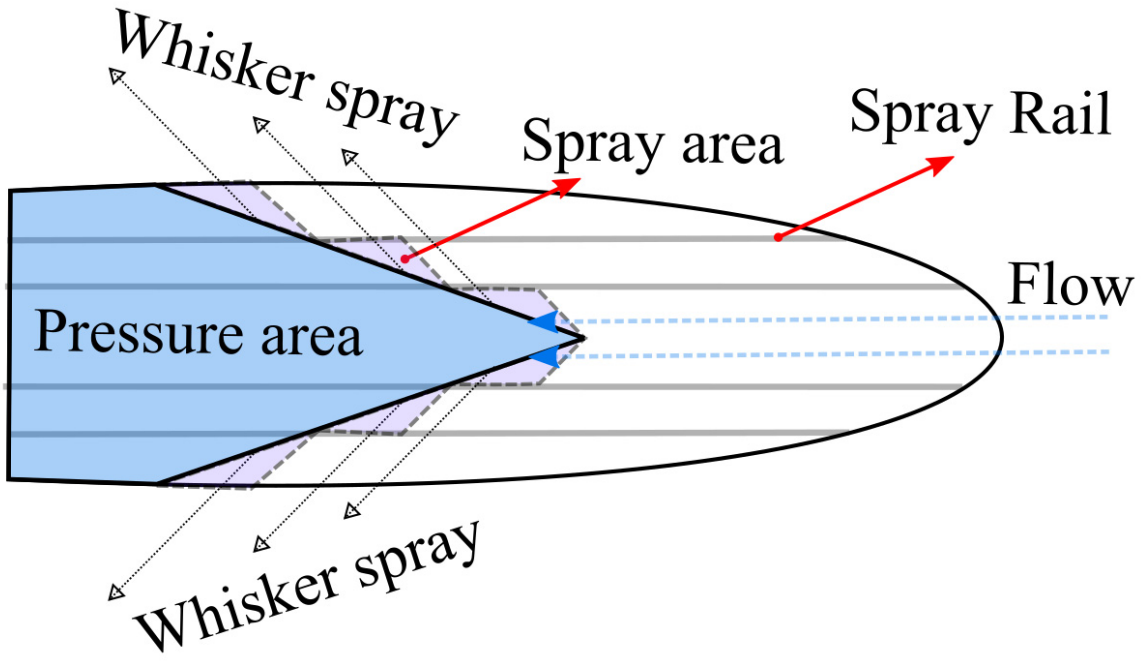


**Figure 2.** Illustration the effect of adding longitudinal spray rails on whisker spray regions generated by a prismatic model planing hull, adapted from Clement [9].

*Model Study and Spray Rail Modification*

In this research, the parent hull (C1) from the Naples Systematic Series (NSS) is used as the reference model [28]. Table 1 lists the main parameters of the hull. The choice of a triangular cross-section for the spray rails (SR) is based on its demonstrated ability to effectively redirect flow away from the hull while generating lift, as shown in Figure 2. The triangular shape is particularly suited for minimizing resistance and controlling the flow of water around the hull, as supported by previous studies [12,30]. In Figure 3, the spray rail's cross-sectional characteristics are labeled as A, B, and C, with the bottom angle denoted by δ.

**Table 1.** Principal characteristics of C1 hull.

| Parameters | Description | Values | Units |
|---|---|---|---|
| $L_{WL}$ | Waterline length | 2.4 | m |
| $B_{WL}$ | Waterline beam | 0.743 | m |
| $T$ | Draft | 0.167 | m |
| Δ | Displacement | 106.7 | Kg |
| τs | Static trim | 0 | Deg |
| $S_{WS}$ | Static-wetted surface area | 1.7 | $m^2$ |
| L/B | Length-to-beam ratio | 3.23 | NIL |

Spray rails (SRs) play a crucial role as previous studies have explored various spray rail shapes and designs [31].

Key design parameters influencing SR effectiveness include the spray rail angle (δ), its width (bSR, denoted as "AC" in Figure 3 and Table 2), and its length (LSR). Muller-Graf [30] established criteria for these parameters, suggesting that the spray rail width should be approximately 0.5% of the hull's waterline length. For the C1 hull, this corresponds to a width of 12 mm, closely matching the SR4 configuration, which measures 11.55 mm (0.48% of *LWL*). Other variations, such as SR1 through SR3 (0.72% of *LWL*) and SR5 through SR7 (0.96% of *LWL*), feature increased widths to investigate the effect of larger spray rails on resistance.

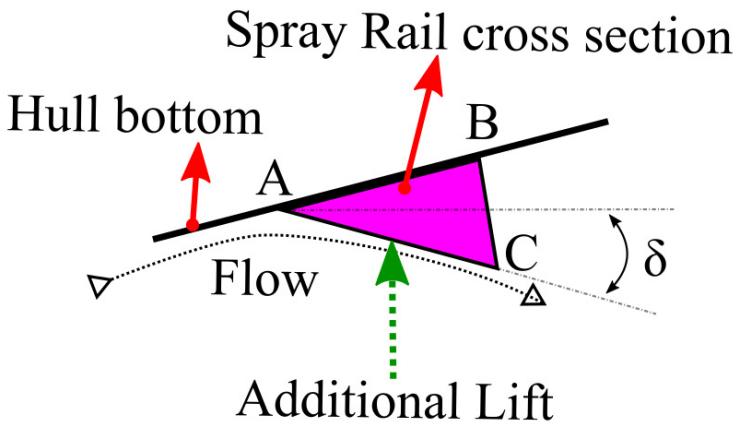


**Figure 3.** Depiction of spray rail fluid flow, showing how it redirects flow away from the hull while simultaneously generating lift. The spray rail's cross-sectional characteristics are labeled as A, B, and C. The bottom angle of the spray rail is denoted by δ.

**Table 2.** Spray rail's dimensions details.

| SRs Design | AB (mm) | BC (mm) | AC (mm) | δ (Deg) |
|---|---|---|---|---|
| SR1-N3 | 15 | 8.66 | 17.32 | 15.61 |
| SR2-N2 | 15 | 8.66 | 17.32 | 15.61 |
| SR3-N1 | 15 | 8.66 | 17.32 | 15.61 |
| SR4-N3S | 10 | 5.77 | 11.55 | 15.61 |
| SR5-N3L | 20 | 11.55 | 23.09 | 15.61 |
| SR6-N3-NK | 20 | 11.55 | 23.09 | 15.61 |
| SR7-N3-NC | 20 | 11.55 | 23.09 | 15.61 |

Crucially, the placement of spray rails is equally important. The leading edge must extend forward of the stagnation line to manage initial spray at low speeds, and at high speeds, the rails should reach forward to any step to prevent chine walking. Table 2 and Figure 4 detail the dimensions and placements of the spray rails, showing the diversity in configurations tested.

This study evaluates seven distinct SR arrangements, each varying in size, position, and quantity (Table 3). The configurations range from SR1-N3 to SR3-N1, with the number of rails decreasing from six to two. Furthermore, SR4-N3S and SR5-N3L explore the smallest and largest spray rail dimensions, while SR6-N3K and SR7-N3C investigate the effects of positioning the rails closer to the keel and chine, respectively. Full-length spray rails were chosen to maximize the spray deflection, increase lift, and reduce wetted surface area, collectively leading to enhanced hydrodynamic efficiency.

**Table 3.** SRs configurations details.

| SRs Design | Shape | No. of SRs | Arrangement |
|---|---|---|---|
| SR1-N3 | Triangular | 3 | Three rails |
| SR2-N2 | Triangular | 2 | Two rails |
| SR3-N1 | Triangular | 1 | One rail |
| SR4-N3S | Triangular | 3 | Smaller size |
| SR5-N3L | Triangular | 3 | Larger size |
| SR6-N3-NK | Triangular | 3 | Near keel position |
| SR7-N3-NC | Triangular | 3 | Near chine position |

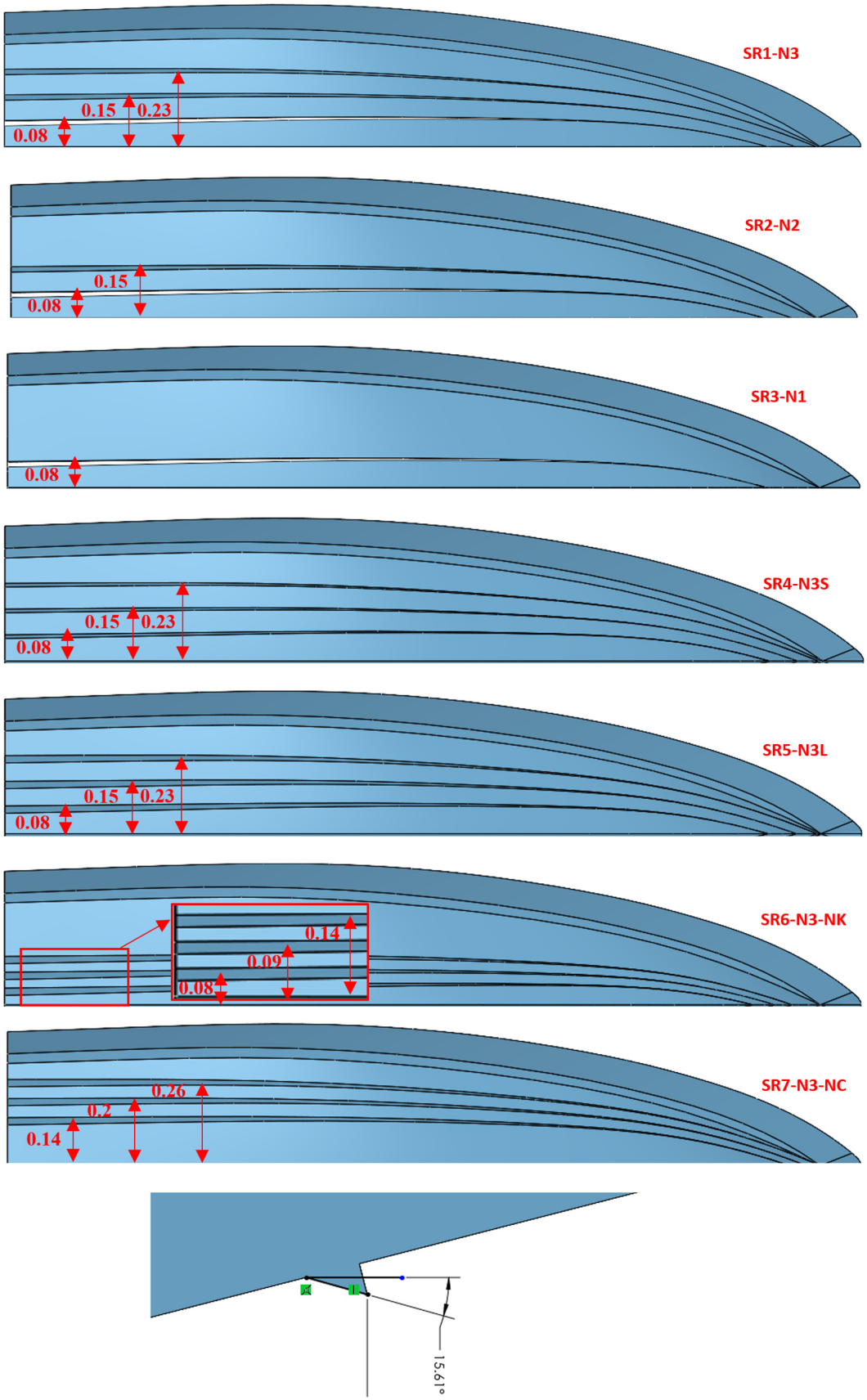


**Figure 4.** Cross-sections and arrangement of spray rails on the C1 hull, showing variations in number, size, and position relative to the keel and chine.

By systematically analyzing these variations, this study aims to uncover the optimal spray rail configuration for minimizing resistance and effectively managing whisker spray on planing hulls.

## 3. Numerical Model

The planing hull hydrodynamics simulations in this study utilized the commercial CFD software STAR-CCM+ [29]. The governing equations were the Reynolds-averaged Navier–Stokes equations (RANSE), which model the conservation of mass and momentum for incompressible fluid flow. The assumption of incompressibility implies constant fluid density, and the governing equations are as follows:

$$\frac{\partial(\rho\overline{u}_i)}{\partial x_i} = 0 \text{ (Conservation of Mass)} \tag{1}$$

$$\frac{\partial(\rho\overline{u}_i)}{\partial t} + \frac{\partial}{\partial x_j}\left(\rho\overline{u}_i\overline{u}_j + \rho\overline{u'_i u'_j}\right) = -\frac{\partial\overline{p}}{\partial x_i} + \frac{\partial\overline{\tau}_{ij}}{\partial x_j} \text{(Conservation of Momentum)} \tag{2}$$

$$\overline{\tau}_{ij} = \mu\left(\frac{\partial\overline{u}_i}{\partial x_j} + \frac{\partial\overline{u}_j}{\partial x_i}\right) \text{(Viscous Stress Tensor)} \tag{3}$$

where $\rho$ is density, $\overline{u}_i$ represents the averaged V Cartesian components of velocity vector, $\rho\overline{u'_i u'_j}$ denotes the Reynolds stresses, accounting for the effects of turbulence, $\overline{\tau}_{ij}$ is the viscous stress tensor, and $\mu$ is the dynamic viscosity. Readers seeking a deeper understanding of these governing equations can refer to works such as Ferziger et al. [32] or Reynolds [33].

To solve these equations, an implicit unsteady solver was employed using a segregated flow approach. The volume of fluid (VOF) method, combined with high-resolution interface capturing (HRIC), was implemented to accurately model the interactions between the air and water phases.

The hull was allowed two degrees of freedom—heave and pitch—via the dynamic fluid–body interaction (DFBI) framework. The SIMPLE algorithm (semi-implicit method of pressure-linked equations) was applied for pressure-velocity coupling, ensuring the robust treatment of fluid–body interactions. The realizable k–$\epsilon$ turbulence model, combined with wall functions, was used to close the RANS equations. Near-wall mesh thickness (y) was calculated using ITTC recommendations [34], with y+ maintained between 30 and 300 for accurate wall function application. Details about the y+ values can be found in Appendix A, Figure A1.

Overset mesh technology enabled fine-resolution meshing around the hull, and time-dependent simulations adhered to ITTC [34] guidelines for time step selection:

$$\Delta t = 0.005 \sim 0.01\frac{LWL}{V} \tag{4}$$

For a hull waterline length ($LWL$) of 2.4 m and maximum speed ($V$) of 8 m/s, the time step $\Delta t$ = 0.005 s was chosen, balancing computational efficiency with accuracy.

The numerical methods and solver details are further elaborated in the Siemens PLM Star-CCM+ User Guide [29]. Additional simulation settings, fluid properties, and computational parameters are provided in Table 4.

**Table 4.** Solver settings.

| Item | Settings |
|---|---|
| Solver | Implicit unsteady |
| Convection term | 2nd order |
| Temporal discretization | 1st order |
| Time-step | As detailed in Equation (4) |
| Inner iterations per time step | 5 |
| Turbulence model | Realizable k-ε |
| Overset interpolation scheme | Linear |
| Wall treatment | All y+ wall treatment |
| Number of prism layers | 9 |
| Prism layer thickness | 0.02 m |
| NV treatment | VOF source control, [35,36] |
| DFBI | Free motion |
| DOF | 2DOF: Pitch and heave |
| Water density | 997.5 kg/m$^3$ |
| Water viscosity | 0.00088 Pa-s |
| Air density | 1.184 kg/m$^3$ |
| Air viscosity | 0.0000185 Pa-s |

*Boundary Condition and Fluid Domain*

In this simulation study, a rectangular fluid domain was established along the x, y, and z axes. The assigned boundary types included velocity inlets, a pressure outlet, a symmetry plane, and walls. The front, top, sides, and bottom boundaries were designated as velocity inlets, while the rear boundary served as the pressure outlet. Wall boundary conditions were applied to the hull surfaces, including the deck, stern, and bottom. To mitigate wave reflections and interference at the far-field boundaries, the wave damping condition was implemented at the outlet.

An overset mesh technique was employed at the interface between the moving hull region and the stationary (background) region.

The dimensions of the fluid(s) domain and the overset box, as illustrated in Figure 5, were determined based on key hull parameters: Lpp (length between perpendiculars), D (Depth), and B (Beam). A symmetry boundary approach was adopted, simulating only half of the hull, which significantly reduced the computational costs while maintaining accuracy.

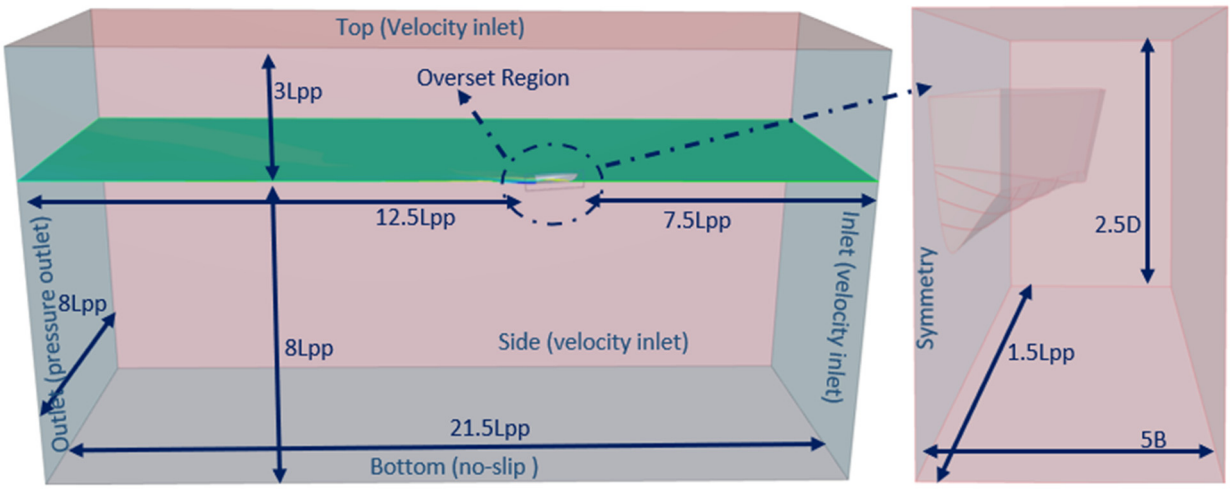


**Figure 5.** Computational fluid domain shows the overset region and corresponding dimensions, highlighting the relationship between the fluid boundaries and the hull geometry.

## 4. Preliminary Analysis

### 4.1. Verification Study: Mesh Independence and Uncertainty

The verification process focused on ensuring numerical accuracy and reliability by addressing mesh independence and quantifying uncertainty. Five grid configurations, ranging from coarse to fine (Grid 0 to Grid 4), were analyzed to balance computational cost and accuracy. The mesh refinement was concentrated on critical regions like the bow, free surface, and overset area, as illustrated in Figure 6 which is captured from the SR6 case, and the six other SRs cases have the same type of refinement.

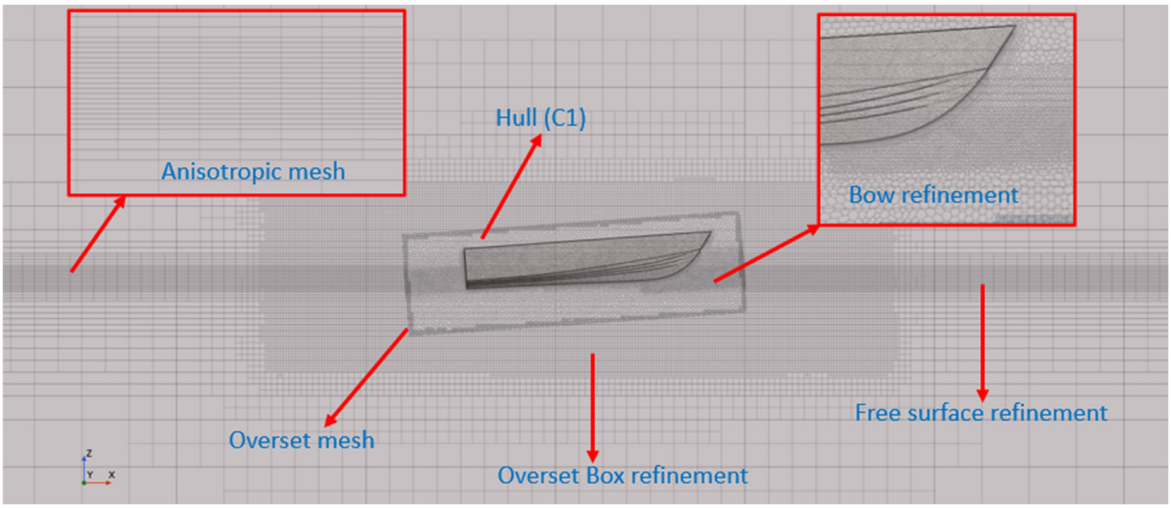


**Figure 6.** Visualization of the background and overset regions, highlighting the mesh refinements in critical areas of the fluid domain, including the bow, free surface, and overset region, to enhance accuracy and resolution in hydrodynamic simulations.

A hybrid meshing approach was adopted, using the trimmer mesh for the background and polyhedral mesh for the overset zone. This strategy reduced the computational time while maintaining the result accuracy, aligning with the best practices outlined by De Luca et al. [35]. After assessing the results, Grid 1 was selected as optimal, as it delivered near-experimental accuracy with minimal computational expense. Table 5 and Figure 7 present the results showcasing minor variations in $R_T/\Delta$ values across grids, reinforcing this selection.

**Table 5.** Mesh independence study.

| Grids | $Fr_\nabla$ | Element Count | Resistance ($R_T/\Delta$) |
|---|---|---|---|
| Grid 0 | 1.42 | $7.07 \times 10^5$ | 0.1101 |
| Grid 1 | 1.42 | $1.00 \times 10^6$ | 0.1104 |
| Grid 2 | 1.42 | $1.41 \times 10^6$ | 0.1097 |
| Grid 3 | 1.42 | $2.00 \times 10^6$ | 0.1099 |
| Grid 4 | 1.42 | $2.86 \times 10^6$ | 0.1101 |

The refinement ratio grids were maintained equal to $\sqrt{2}$, following ITTC guidelines [37]. Overset mesh refinement ensured a uniform donor–acceptor distribution for consistency in hydrodynamic evaluations [29].

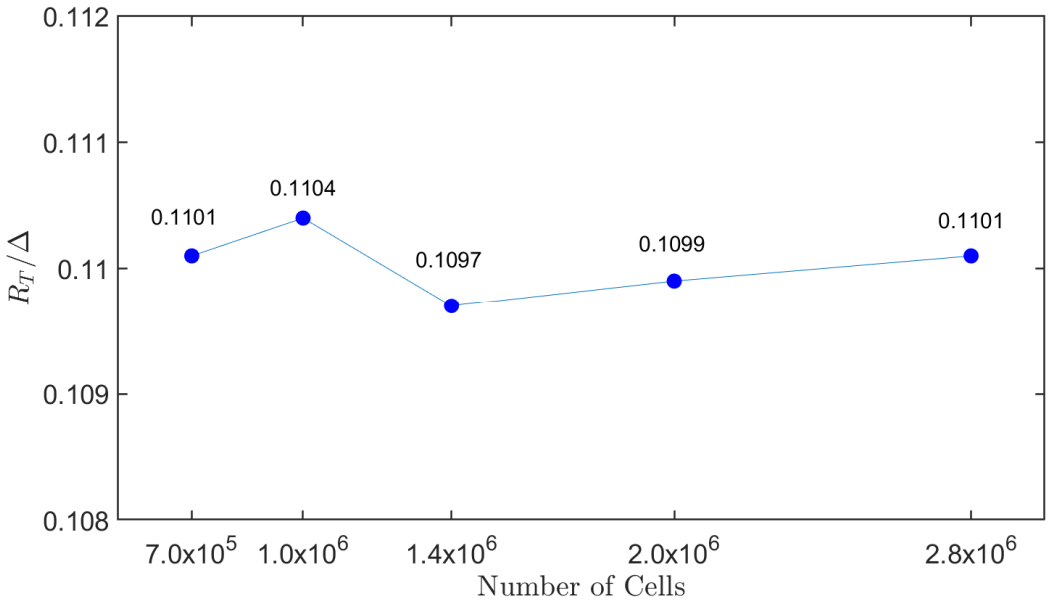


**Figure 7.** Results of the mesh independence study, illustrating the effect of grid refinement on the accuracy of hydrodynamic simulations, with a focus on achieving an optimal balance between computational efficiency and solution precision.

To quantify uncertainty, the discretization error (U) was calculated using Richardson extrapolation [38]. The uncertainty equation used is:

$$U = F_s|\delta_{RE}| \tag{5}$$

$F_s$ is a factor of safety and $\delta_{RE}$ is Richardson extrapolation error, calculated as:

$$\delta_{RE} = \varnothing_i - \varnothing_o = \alpha h_i^p \tag{6}$$

where $\varnothing_i$ is numerical solution on a given grid, $\varnothing_o$ is extrapolated exact solution, $h_i$ is grid cell size parameter, $p$ is the order of accuracy, and $\alpha$ is a constant determined through least squares.

The least-squares method minimized the error function $S(\varnothing_o, \alpha, p)$, defined as:

$$S(\varnothing_o, \alpha, p) = \sqrt{\sum_{i=1}^{n_g}(\varnothing_i - (\varnothing_o + \alpha h_i^p))^2} \tag{7}$$

For the standard deviation of uncertainty, the formula used was:

$$U_s = \sqrt{\frac{\sum_{i=1}^{n_g}(\varnothing_i - (\varnothing_o + \alpha h_i^p))^2}{n_g - 3}} \tag{8}$$

here, $n_g$ represents the number of grid levels used in the grid convergence study which in this case is (A, B, C, D, and E). The convergence type is determined based on the $p$ value. Monotonic convergence occurs when $p > 0$, monotonic divergence when $p < 0$, oscillatory divergence when $p^* < 0$, and oscillatory convergence otherwise; the $p_G$ is calculated as 1.09. Details regarding this approach are discussed in Eça and Hoekstra [39] and ITTC 75-03-01-01 Rev 04 [37]. The grid uncertainty analysis results for the finest grid at $Fr_\nabla$ = 1.42 are presented in Table 6. These results quantify the uncertainty associated with the grid ($U_G$) for a specific parameter, expressed as a percentage of parameter value related to the finest grid case.

**Table 6.** Grid uncertainty result for hull resistance at $Fr_{\nabla} = 1.42$ ($U_G$ expressed as percentage related to the finest grid).

| Refinement Ratio | $p_G$ | $U_G$ ($R_T/\Delta$) |
|---|---|---|
| 1.41 | 1.09 | 0.80% |

*4.2. Comparison with Experimental Data*

To validate the numerical model, the results were compared against experimental data for the Naples Systematic Series (NSS) parent hull (C1) [28]. The comparison was performed at $Fr_{\nabla}$ = 1.42, 2.79, and 3.26 for resistance, wetted surface area, and dynamic trim as shown in Table 7.

**Table 7.** Shows the percentage error of comparison between CFD and EFD results.

| $Fr_{\nabla}$ | Total Resistance (%) | Dynamic Trim (%) | Wetted Surface Area (%) |
|---|---|---|---|
| 1.42 | −5.34 | −12.44 | 10.39 |
| 2.79 | −4.22 | −7.09 | 2.52 |
| 3.26 | −2.09 | −9.53 | 25.49 |

The results demonstrated excellent agreement, with resistance errors below 5% and dynamic trim errors within 10–15%, matching the ITTC standards [34]. Small discrepancies at $Fr_{\nabla}$ = 1.42 were attributed to coarser mesh and larger time steps at lower speeds, which could be refined but at a higher computational cost. The numerical model performed well at higher speeds, where the focus of the study lies.

The deviations in the wetted surface area were attributed to unaccounted whisker spray in the experimental data [28] and are comparable with the calculated wetted surface values show in the study of De Luca et al. [35]. However, these discrepancies did not impact on the study's overall conclusions on resistance reduction and high-speed performance.

## 5. Results

The NSS parent hull (C1) was selected for modifications with spray rails. The validation of the numerical setup was discussed in the previous section. Simulations were carried out for three volumetric Froude numbers: 1.42, 2.79, and 3.26. The results focus on the dimensionless resistance, wetted surface, sinkage, and dynamic trim, which are graphically represented in Figures 8–11. Detailed data can be found in Appendix B, Tables A1–A3. To ensure a comprehensive analysis of the impact of spray rail quantity, size, and position, modifications were made to the base hull configuration. All simulations were conducted with an unsteady solver using a mesh of approximately 1 million elements.

Figure 8 shows the dimensionless resistance values for the seven hull modifications at the three Froude numbers, illustrating their hydrodynamic performance. At lower Froude numbers, the spray rail configurations exhibit slightly higher resistance compared to the base hull. However, as speed increases, the resistance generally decreases for certain configurations. Specifically, the SR5-N3L and SR7-N3-NC configurations demonstrate the lowest resistance values at $Fr_{\nabla}$ = 3.26, indicating that placing the spray rails near the chine contributes to generating lift and reducing resistance at higher speeds. Conversely, other configurations, such as SR6-N3-NK (rails near the keel), exhibit higher resistance across all speeds, highlighting the sensitivity of resistance to spray rail placement.

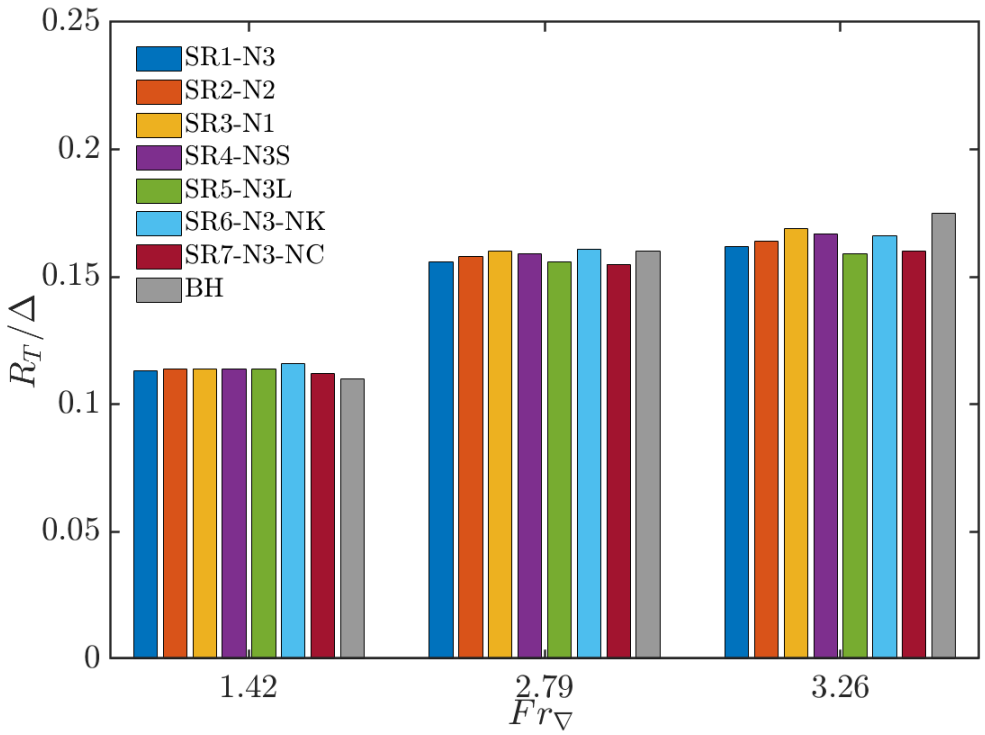


**Figure 8.** Comparison of the CFD results of resistance coefficient for SRs hulls with base hulls.

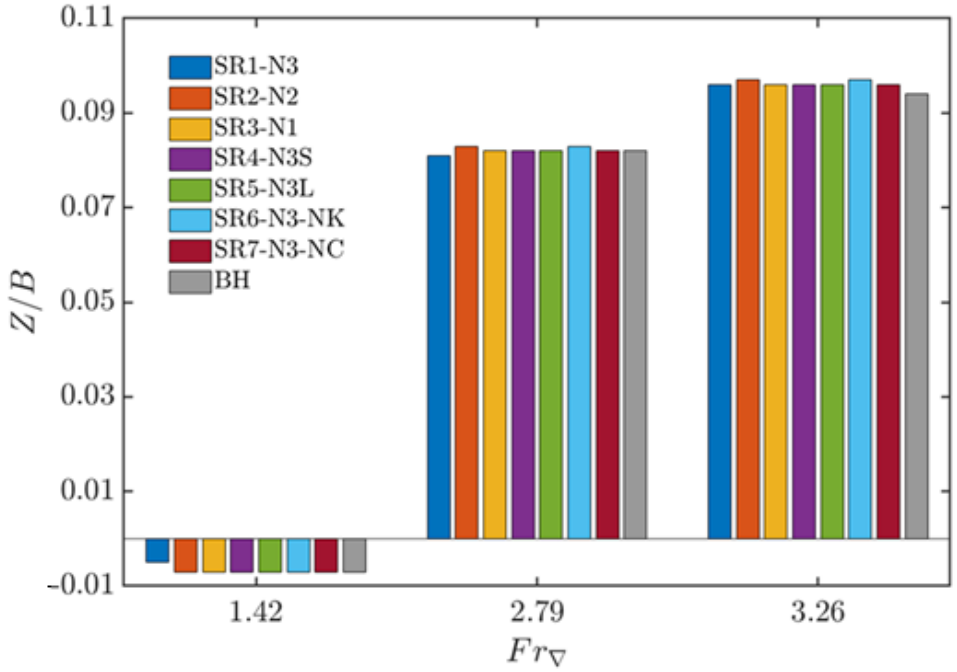


**Figure 9.** Comparison of the sinkage of CFD results for SRs hulls with base hulls.

As the volumetric Froude number increases from 1.42 to 3.26, a trend of rising resistance values is observed for all hull configurations, aligning with expectations that higher speeds lead to increased hydrodynamic resistance. This comparison underscores the importance of optimizing spray rail size and position to achieve reduced resistance and enhanced hydrodynamic performance at high speeds.

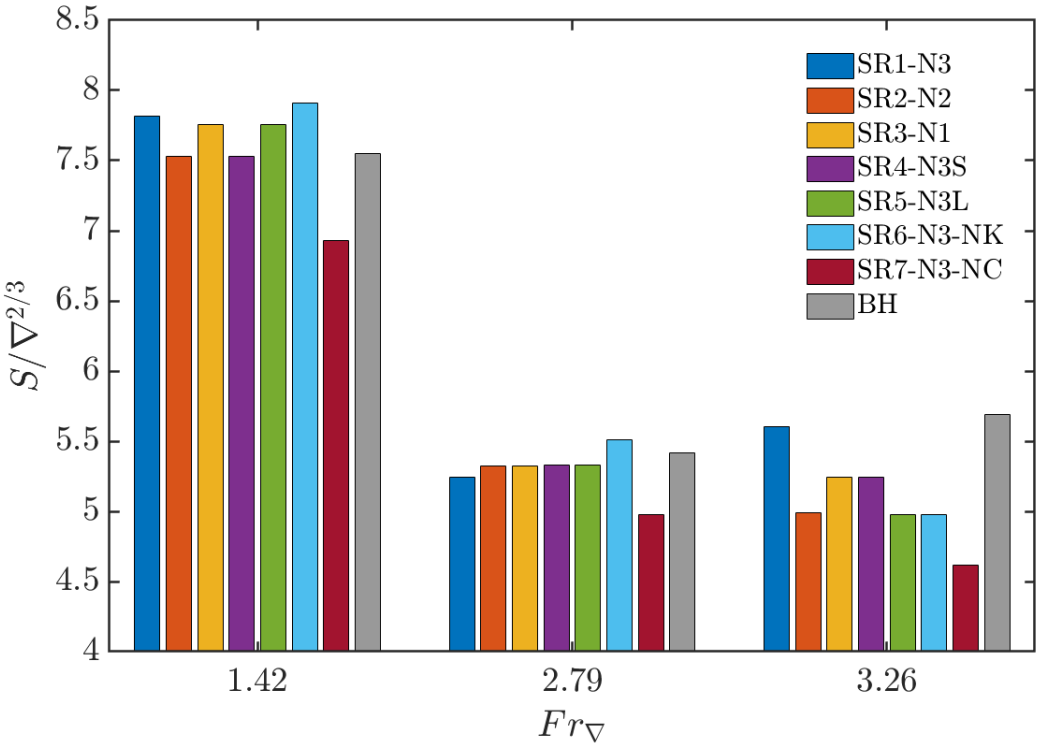


**Figure 10.** Comparison of wetted surface of CFD results for SRs hulls with the base hull.

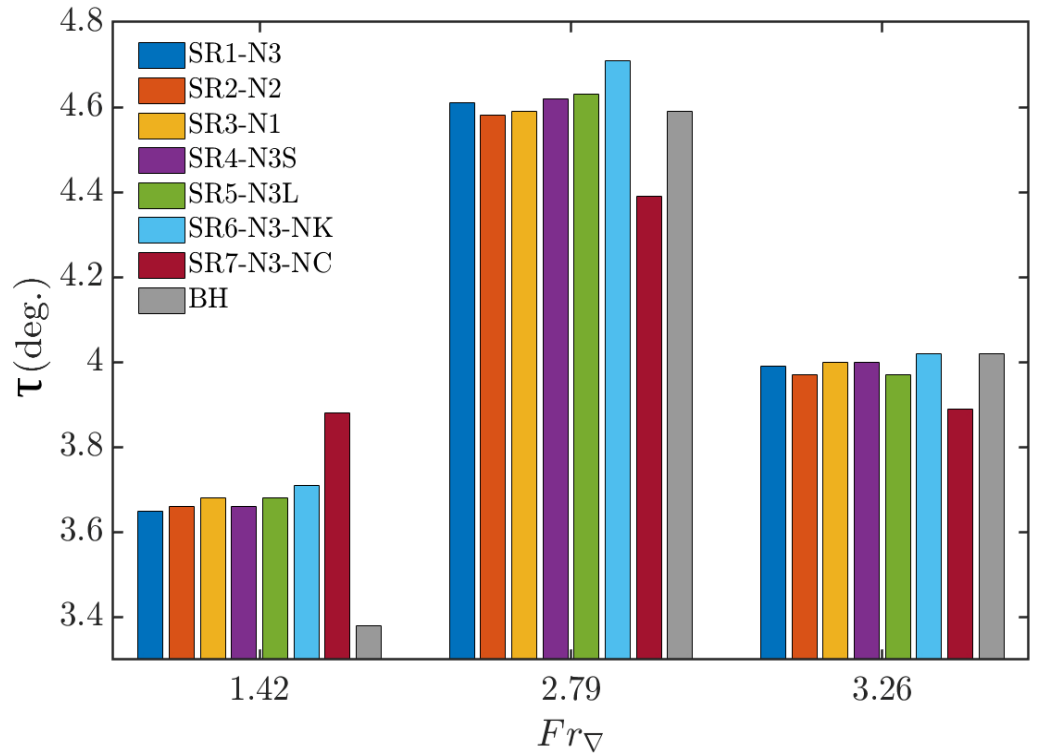


**Figure 11.** Comparison of dynamic trim of CFD results for SRs hulls with the base hull.

Figure 9 shows the sinkage behavior for all hulls at the three tested speeds. At low speeds, the sinkage values for the modified SR hulls remain similar to those of the base hull (BH). However, as speed increases, the sinkage values for the SR hulls begin to rise and exceed those of the base hull, especially at the highest Froude number. At $Fr_\nabla$ = 3.26, the base hull exhibits lower sinkage compared to all the modified hulls. This suggests that

the SR hulls experience greater vertical displacement, meaning they lift more out of the water as speed increases. This increased lift contributes to the reduction in wetted surface area, which in turn reduces the hydrodynamic resistance. In essence, higher sinkage values correspond to a hull that is more out of the water, benefiting the performance by reducing wetted surface and subsequently resistance.

In continuation of the results from Figure 9 (sinkage plot), Figure 10 presents a detailed comparison of the wetted surface area, normalized by the hull's characteristic volume ($S/\nabla^{2/3}$), for the various hull configurations. The wetted surface area is a key factor in resistance performance, as a reduction in wetted surface directly leads to decreased resistance.

At lower speeds ($Fr_{\nabla}$ = 1.42), the wetted surface remains relatively consistent across all hulls. However, as speed increases, the distinction between hull configurations becomes more pronounced. At $Fr_{\nabla}$ = 2.79, the SR6 configuration shows a higher wetted surface than the base hull (BH), implying that its design might be less effective at reducing drag at this speed. Conversely, SR7-N3-NC, which features six spray rails near the chine, demonstrates the most significant reduction in wetted surface across all speeds. By $Fr_{\nabla}$ = 3.26, SR7 exhibits the lowest wetted surface, outperforming both the base hull and other spray-rail-modified configurations.

The reduction in wetted surface for SR7 results from its rail placement and larger cross-sectional area, particularly near the chine. This design effectively lifts the hull out of the water at higher speeds, reducing both wetted surface and resistance, making SR7 the most efficient configuration in terms of hydrodynamic performance. The decrease in wetted surface observed with increasing speed highlights the efficiency of well-placed spray rails in improving the overall performance of planing hulls.

Following the analysis of the wetted surface, Figure 11 illustrates the dynamic trim results for all configurations, offering insights into how each hull design performs at various speeds. Trim is a critical factor in high-speed craft performance as it affects both resistance and the onset of porpoising. Although this study primarily focuses on the hydrodynamic benefits of spray rails, it is important to note that trim changes are often a side effect of hull modifications like spray rails, steps, or interceptors.

As shown in Figure 11, the dynamic trim angles are relatively consistent across all configurations, with only slight variations at different Froude numbers, except for the BH and SR7-N3-NC cases. This indicates that the SR7-N3-NC configuration has an impact on the trim that is related to the center of pressure position modified by the spray rails configuration. Notably, while the main function of spray rails is to deflect water away from the hull and reduce wetted surface, their placement might also influence trim in subtle ways, although not to a significant degree in this study for all cases. The uniformity of trim across configurations suggests that the primary role of the rails here is to manage spray rather than alter the trim angle.

### *5.1. Volume of Fraction*

The volume of fraction (VOF) method is employed to quantify and analyze the wetted surface area. This multiphase simulation approach assigns values between 0 and 1, where 0 represents air and 1 represents water. The interface between air and water is modeled at the hull's bottom surface, as depicted in Figure 12.

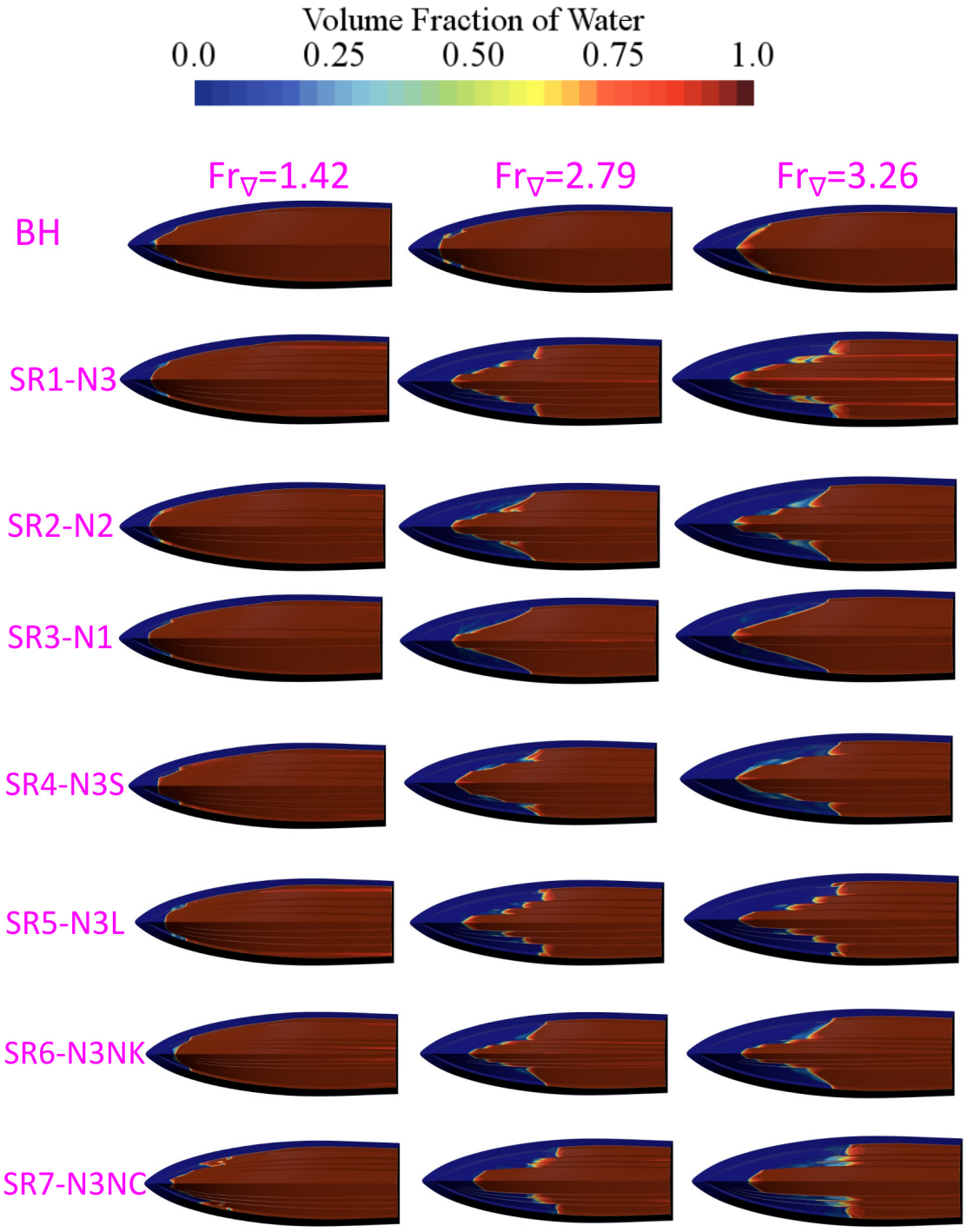


**Figure 12.** Volume of fraction of SR hull and base hull at three beam Froude number.

As speed increases, the wetted surface area decreases due to the generation of dynamic lift, which raises the hull and reduces its contact with the water surface. However, spray rails act as flow deflectors, disrupting water adhesion and directing the spray away from the hull surface. This redirection minimizes stagnation pressure at the hull-water interface, reduces resistance, and improves hydrodynamic efficiency. Additionally, spray rails contribute to lift generation (and the center of pressure position along the hull bottom) by modifying the pressure distribution along the hull, further enhancing performance, especially at higher speeds, where their impact on drag reduction and whisker spray minimization becomes more pronounced.

A notable issue arises in the CFD simulations of high-speed crafts where the free surface is modeled using the VOF approach. This is called numerical ventilation, which is a phenomenon where air becomes trapped within the boundary layer near the water surface and is transported to submerged regions, which complicates simulations. This trapped air, although forming a small fraction of the boundary layer, significantly impacts shear stress calculations. Incorrect calculations occur because the fluid in this mixed region does not exhibit purely water-like properties.

To address the numerical ventilation problem, in this study, a VOF suppression technique is implemented, identifying and modifying cells affected by ventilation to exclude the air fraction in these cells. This method minimizes numerical diffusion and improves accuracy. Comparative studies, such as those by Viola et al. [36], highlight the advantages of this approach over conventional methods like the standard and modified HRIC schemes, as detailed by De Luca et al. [35].

The analysis revealed that, at lower speeds, spray rails can slightly increase resistance due to increased wetted surface area. However, at higher speeds, particularly at $Fr_{\nabla} = 3.26$, a significant reduction in wetted surface area and resistance was achieved. This reduction is primarily attributed to the decreased whisker spray facilitated by spray rail configurations. Among the configurations tested, the SR7 demonstrated the lowest resistance across all speeds, making it the most efficient design in terms of hydrodynamic performance. This suggests that positioning the spray rail closer to the chine has a profound impact on minimizing whisker spray. The closer proximity redirects water more effectively, reducing the wetted surface area and improving overall craft efficiency.

### *5.2. Pressure Coefficient Distribution Contours*

At higher speeds, vessels transition from being influenced primarily by hydrostatic forces at lower speeds to hydrodynamic forces that dominate their behavior. The way pressure is distributed along the hull, especially around the stagnation line, plays a crucial role in shaping the vessel's performance.

Pressure coefficient contours provide insights into this distribution, as shown in Figure 13. High-pressure areas, represented in red near the stagnation line, indicate regions where fluid slows down, leading to increased resistance. Conversely, low-pressure zones, shown in blue near the stern, promote smoother flow and help reduce drag.

Increased resistance and inefficient pressure distribution control on the hull bottom are observed in hulls without spray rails. In contrast, hulls equipped with spray rails (SR1-N3 to SR7-N3-NC) exhibit a more uniform pressure distribution. Spray rails help reduce the intensity of the stagnation line and the high-pressure zone around it, minimizing the effect of whisker spray and ultimately leading to lower drag. They also enhance the lift, move the center of pressure along the hull bottom, and reduce the wetted surface at higher speeds, improving the overall performance.

Furthermore, spray rails create localized high-pressure zones along the hull edges. These zones contribute to lift by directing water flow downward, acting on the hull dynamic sinkage and trim. The combination of smoother pressure distribution, increased lift, and reduced drag highlights how spray rails significantly enhance vessel performance, particularly at high speeds.

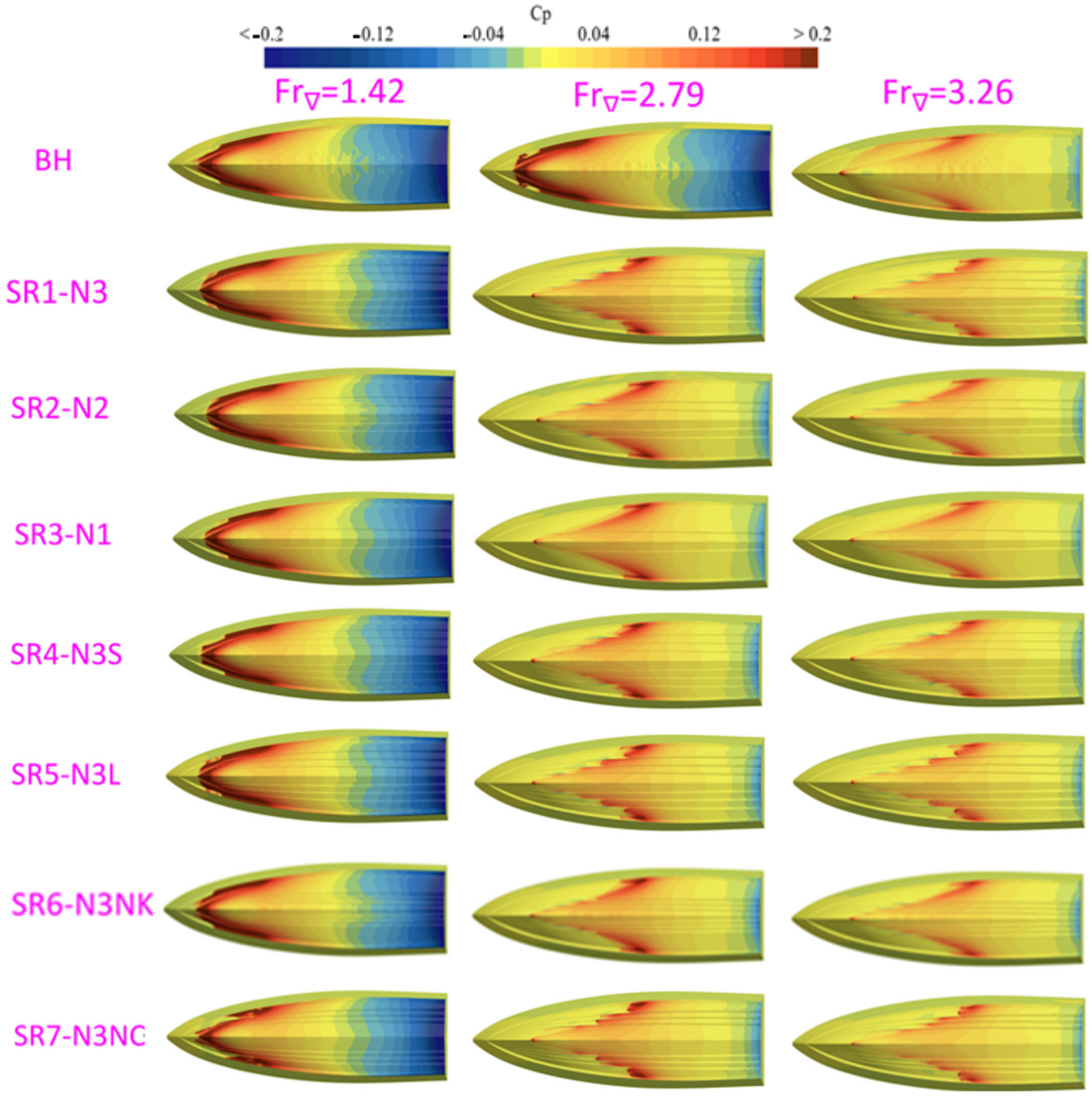


**Figure 13.** Pressure coefficient contours illustrating the pressure distribution on the base hull (BH) and spray rail-equipped hulls (SRs) at three different volumetric Froude numbers. The comparison highlights the impact of spray rails on reducing high-pressure zones near the stagnation line and improving overall hydrodynamic efficiency.

## 6. Conclusions

This study investigated the effects of spray rails (SRs) on the hydrodynamic performance of the C1 hull Naples Systematic Series (NSS), aiming to identify the most effective configurations regarding size, number, and positioning. The findings highlight the ability of spray rails to reduce whisker spray, minimize wetted surface area, and lower overall resistance at higher speeds. While the effect in dynamic trim was not substantial across all speeds, the primary function of SRs was observed to be the wetted surface area reduction. The rails also generated lift, and due to their variable cross-sectional size from stern to bow, uneven lift distribution resulted in a changing of center of pressure and a consequently changing of dynamic trim, with an approximately 3% rise noted at high speeds.

A significant focus was placed on the design of SRs, including variations in number, location, and size. Three SR widths—0.48%, 0.72%, and 0.96% of the *LWL*—were studied, with a constant rail angle of 15.61°. Wider SRs, such as SR7 (0.96% *LWL*), effectively reduced resistance at high speeds (up to 8.5% compared to the base hull) but slightly increased resistance at lower speeds (approximately 2%) due to a larger wetted surface. The

placement of spray rails proved critical; SRs positioned near the chine (e.g., SR7) were more effective than those near the keel (e.g., SR6), achieving a 4% greater reduction in resistance.

The number of spray rails also influenced hydrodynamic performance. Configurations with multiple SRs per side (e.g., SR1 with three rails) achieved a 4% resistance reduction compared to SR3, which had only one rail. These findings emphasize the importance of optimizing the number, position, and size of SRs based on specific operating conditions. Using two to three spray rails per side, strategically placed near the chine, is recommended for achieving optimal performance.

This research used full-length spray rails for all configurations; however, future studies could investigate variable-length rails to explore potential performance enhancements. Prior research on the C1 hull incorporating steps showed significant resistance reduction [40], suggesting that a combination of steps and spray rails might offer synergistic benefits.

In conclusion, this study highlights the significant role of spray rails in optimizing hydrodynamic performance, particularly for high-speed vessels. The insights gained provide a strong foundation for further exploration into SR design, ensuring better efficiency and performance across a range of operating conditions.

**Author Contributions:** Conceptualization, M.S.; methodology, M.S., S.M. and R.N.B.; software, M.S. and R.N.B.; validation, S.M. and M.S.; formal analysis, M.S., S.M. and R.N.B.; investigation, M.S. and S.M.; resources, S.M. and L.V.; data curation, M.S. and R.N.B.; writing—original draft preparation, M.S., S.M. and R.N.B.; writing—review and editing, S.M., R.N.B. and L.V.; visualization, M.S. and R.N.B.; supervision, S.M. and R.N.B.; project administration, L.V.; funding acquisition, L.V. All authors have read and agreed to the published version of the manuscript.

**Funding:** This research received no external funding.

**Institutional Review Board Statement:** Not applicable.

**Informed Consent Statement:** Not applicable.

**Data Availability Statement:** Data will be available upon request to the corresponding author.

**Conflicts of Interest:** The authors declare no conflict of interest.

## Nomenclature and Abbreviations

| | | | |
|---|---|---|---|
| $L_{WL}$ | Waterline length | ITTC | International Towing Tank Conference |
| $B_{WL}$ | Beam waterline | VOF | Volume of fraction |
| $T$ | Draft | DFBI | Dynamic fluid–body interaction |
| $\tau_s$ | Static trim | SIMPLE | Semi-implicit pressure linked equation |
| $\Delta$ | Displacement | CFD | Computational fluid dynamics |
| $^L/_B$ | Length-to-beam ratio | SR | Spray rail |
| $\nabla$ | Volume | NSS | Naple Systematic Series |
| $\delta$ | Spray rail angle | HRIC | High resolution |
| $\Delta t$ | Time Step | RANS | Reynolds-averaged Navier–Stoke equation |
| $Fr_\nabla$ | Volumetric Froude number | | |
| $C_p$ | Pressure coefficient | | |
| z | Sinkage | | |
| $S_{WS}$ | Static wetted surface area | | |

## Appendix A. Wall Y+

The wall y+ is a non-dimensional value that determines the distance between the wall and the first cell of the mesh. It plays an important role in identifying simulation accuracy, it helps to find whether the first mesh cell lies in a viscous sublayer, buffer layer, or logarithmic

region. The recommended wall y+ should be between 30 and 100 for the accurate prediction of results. In this study, the wall y+ is within the range shown in Figure A1 at $Fr_{\nabla} = 3.26$, which is accomplished with proper mesh refinement, especially the critical regions such as bow, stern, and spray rail area that should have more refined mesh.

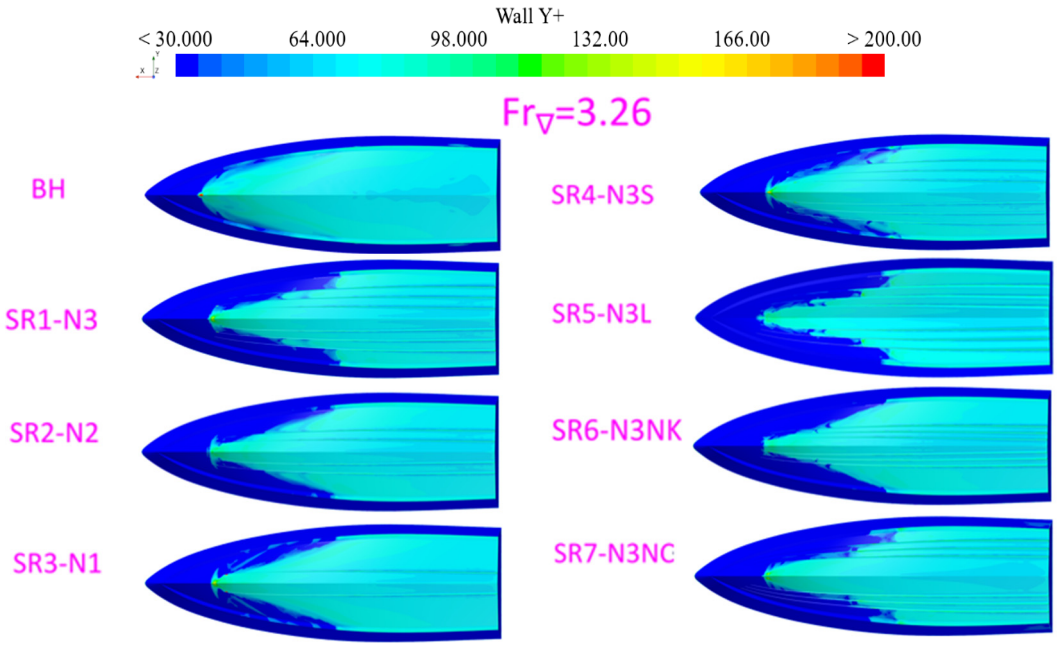


**Figure A1.** Wall Y+ of SRs hull and base hull at $Fr_{\nabla}$ = 3.26.

## Appendix B. CFD Simulations Results

**Table A1.** CFD results at $Fr_{\nabla}$ =3.26.

| SRs Designs | $Fr_{\nabla}$ | Dynamic Trim (Deg.) | Resistance ($R_T/\Delta$) | Wetted Surface ($S/\nabla^{2/3}$) | Sinkage ($z/B$) |
|---|---|---|---|---|---|
| SR1-N3 | 3.26 | 3.99 | 0.162 | 5.065 | 0.096 |
| SR2-N2 | 3.26 | 3.98 | 0.164 | 4.887 | 0.097 |
| SR3-N1 | 3.26 | 3.97 | 0.169 | 5.242 | 0.096 |
| SR4-N3S | 3.26 | 4 | 0.167 | 5.242 | 0.096 |
| SR5-N3L | 3.26 | 4 | 0.159 | 4.976 | 0.098 |
| SR6-N3-NK | 3.26 | 4 | 0.166 | 4.976 | 0.098 |
| SR7-N3-NC | 3.26 | 4.02 | 0.160 | 4.620 | 0.098 |
| BH | 3.26 | 3.89 | 0.175 | 5.687 | 0.094 |

**Table A2.** CFD results at $Fr_{\nabla} = 2.79$.

| SRs Designs | $Fr_{\nabla}$ | Dynamic Trim (Deg.) | Resistance ($R_T/\Delta$) | Wetted Surface ($S/\nabla^{2/3}$) | Sinkage ($z/B$) |
|---|---|---|---|---|---|
| SR1-N3 | 2.79 | 4.61 | 0.156 | 5.242 | 0.083 |
| SR2-N2 | 2.79 | 4.59 | 0.158 | 5.331 | 0.081 |
| SR3-N1 | 2.79 | 4.58 | 0.160 | 5.420 | 0.082 |
| SR4-N3S | 2.79 | 4.62 | 0.159 | 5.331 | 0.082 |
| SR5-N3L | 2.79 | 4.61 | 0.156 | 5.331 | 0.083 |
| SR6-N3-NK | 2.79 | 4.63 | 0.161 | 5.509 | 0.083 |
| SR7-N3-NC | 2.79 | 4.63 | 0.155 | 4.976 | 0.085 |
| BH | 2.79 | 4.59 | 0.160 | 5.420 | 0.082 |

**Table A3.** CFD results at $Fr_{\nabla}$ = 1.42.

| SRs Designs | $Fr_{\nabla}$ | Dynamic Trim (Deg.) | Resistance ($R_T/\Delta$) | Wetted Surface ($S/\nabla^{2/3}$) | Sinkage ($z/B$) |
|---|---|---|---|---|---|
| SR1-N3 | 1.42 | 3.65 | 0.113 | 7.819 | −0.005 |
| SR2-N2 | 1.42 | 3.68 | 0.114 | 7.730 | −0.007 |
| SR3-N1 | 1.42 | 3.68 | 0.114 | 7.553 | −0.007 |
| SR4-N3S | 1.42 | 3.69 | 0.114 | 7.730 | −0.007 |
| SR5-N3L | 1.42 | 3.66 | 0.114 | 7.908 | −0.007 |
| SR6-N3-NK | 1.42 | 3.68 | 0.116 | 7.908 | −0.007 |
| SR7-N3-NC | 1.42 | 3.66 | 0.112 | 6.931 | −0.007 |
| BH | 1.42 | 3.38 | 0.110 | 7.553 | −0.007 |

## References


1. Roshan, F.; Dashtimanesh, A.; Kujala, P. Safety Improvements for High-Speed Planing Craft Occupants: A Systematic Review. *J. Mar. Sci. Eng.* **2024**, *12*, 845. [CrossRef]
2. Niazmand Bilandi, R. Efficient High-Speed Small Craft: Performance in Calm Water and Waves. Ph.D. Thesis, Tallinn University of Technology, Tallinn, Estonia, 2024. [CrossRef]
3. Savitsky, D.; Breslin, J.P. *On the Main Spray Generated by Planing Surfaces*; Report No. 678; Davidson Laboratory, Stevens Institute of Technology: Hoboken, NJ, USA, January 1958.
4. Latorre, R. Study of Prismatic Planing Model Spray and Resistance Components. *J. Ship Res.* **1983**, *27*, 187–196. [CrossRef]
5. Savitsky, D.; DeLorme, M.F.; Datla, R. Inclusion of Whisker Spray Drag in Performance Prediction Method for High-Speed Planing Hulls. *Mar. Technol. SNAME News* **2007**, *44*, 35–56. [CrossRef]
6. Savitsky, D.; Morabito, M. Origin and Characteristics of the Spray Patterns Generated by Planing Hulls. *J. Ship Prod. Des.* **2011**, *27*, 63–83. [CrossRef]
7. Savitsky, D. Hydrodynamic Design of Planing Hulls. *Mar. Technol. SNAME News* **1964**, *1*, 71–95. [CrossRef]
8. Larsson, L.; Raven, H.C. *The Principles of Naval Architecture Series: Ship Resistance and Flow*; Paulling, J.R., Ed.; The Society of Naval Architects and Marine Engineers: Jersey City, NJ, USA, 2010; ISBN 978-0-939773-76-3.
9. Clement, E.P. Reduction of Planing Boat Resistance by Deflection of the Whisker Spray. Department of the Navy: David Taylor Model Basin. 1964. Available online: https://apps.dtic.mil/sti/citations/AD0454407 (accessed on 2 December 2024).
10. Savitsky, D. Planing Craft. *Nav. Eng. J.* **1985**, *97*, 113–141. [CrossRef]
11. Seo, J.; Choi, H.-K.; Jeong, U.-C.; Lee, D.K.; Rhee, S.H.; Jung, C.-M.; Yoo, J. Model tests on resistance and seakeeping performance of wave-piercing high-speed vessel with spray rails. *Int. J. Nav. Archit. Ocean Eng.* **2016**, *8*, 442–455. [CrossRef]
12. Lakatoš, M.; Sahk, T.; Andreasson, H.; Tabri, K. The effect of spray rails, chine strips and V-shaped spray interceptors on the performance of low planing high-speed craft in calm water. *Appl. Ocean Res.* **2022**, *122*, 103131. [CrossRef]
13. Savitsky, D.; Morabito, M. Surface Wave Contours Associated with the Forebody Wake of Stepped Planing Hulls. *Mar. Technol. SNAME News* **2010**, *47*, 1–16. [CrossRef]
14. Garland, W.R. Stepped planing hull investigation. *Soc. Naval Archit. Mar. Eng. (SNAME) Trans.* **2011**, *119*, 448–458.
15. Taunton, D.J.; Hudson, D.A.; Shenoi, R.A. Characteristics of a series of high speed hard chine planing hulls—Part 1: Performance in calm water. *Int. J. Small Craft Technol.* **2010**, *152*, 55–75. [CrossRef]
16. Vitiello, L.; Mancini, S.; Niazmand Bilandi, R.; Dashtimanesh, A.; De Luca, F.; Nappo, V. A comprehensive stepped planing hull systematic series: Part 1—Resistance test. *Ocean Eng.* **2022**, *266*, 112242. [CrossRef]
17. Molchanov, B. Benchmark Testing of Spray Deflection Technologies for High-Speed Planing Craft. Master's Thesis, KTH Royal Institute of Technology, Stockholm, Sweden, 2018. Available online: https://urn.kb.se/resolve?urn=urn:nbn:se:kth:diva-266104 (accessed on 12 January 2025).
18. Molchanov, B.; Lundmark, S.; Fürth, M.; Green, M. Experimental validation of spray deflectors for high speed craft. *Ocean Eng.* **2019**, *191*, 106482. [CrossRef]
19. Wielgosz, C. Experimental Evaluation of Novel Spray Deflector for Planing Hulls. Master's Thesis, KTH Royal Institute of Technology, Stockholm, Sweden, 2018. Available online: https://urn.kb.se/resolve?urn=urn:nbn:se:kth:diva-234903 (accessed on 12 January 2025).
20. Martin, M. Theoretical Prediction of Motions of High-Speed Planing Boats in Waves. *J. Ship Res.* **1978**, *22*, 140–169. [CrossRef]
21. Zarnick, E. A Nonlinear Mathematical Model of Motions of a Planing Boat in Regular Waves; David Taylor Naval Ship Research and Development Center, Technical Report DTNSRDC-78/032. 1978. Available online: https://apps.dtic.mil/sti/citations/ADA052039 (accessed on 15 September 2023).

22. van Deyzen, A.F.J. A nonlinear mathematical model of motions of a planning monohull in head seas. In Proceedings of the 6th International Conference on High-Performance Marine Vehicles, Naples, Italy, 18–19 September 2008; dr Bertorello, C., Ed.; Comitato Organizzatore Hiper 08. 2008; pp. 187–199.
23. Niazmand Bilandi, R.; Mancini, S.; Vitiello, L.; Miranda, S.; De Carlini, M. A Validation of Symmetric 2D + T Model Based on Single-Stepped Planing Hull Towing Tank Tests. *J. Mar. Sci. Eng.* **2018**, *6*, 136. [CrossRef]
24. Niazmand Bilandi, R.; Dashtimanesh, A.; Tavakoli, S. Development of a 2D + T theory for performance prediction of double-stepped planing hulls in calm water. *Proc. Inst. Mech. Eng. Part M J. Eng. Marit. Environ.* **2019**, *233*, 886–904. [CrossRef]
25. Niazmand Bilandi, R.; Dashtimanesh, A.; Tavakoli, S. Stepped Hulls Early Stage Design by Implementing 2D + T Method. In *HSMV 2023*; IOS Press: Amsterdam, The Netherlands, 2023; pp. 23–32. [CrossRef]
26. Cui, L.; Chen, Z.; Feng, Y.; Li, G.; Liu, J. An improved VOF method with anti-ventilation techniques for the hydrodynamic assessment of planing hulls-Part 2: Applications. *Ocean Eng.* **2021**, *237*, 109505. [CrossRef]
27. Tavakoli, S.; Zhang, M.; Kondratenko, A.A.; Hirdaris, S. A review on the hydrodynamics of planing hulls. *Ocean Eng.* **2024**, *303*, 117046. [CrossRef]
28. De Luca, F.; Pensa, C. The Naples warped hard chine hulls systematic series. *Ocean Eng.* **2017**, *139*, 205–236. [CrossRef]
29. *SIEMENS PLM STAR CCM+ User's Guide*, Version 18.04.008; Siemens: Munich, Germany, 2023.
30. Muller-Graf, B. The effect of an advanced spray rail system on resistance and development of spray of semi-displacement round bilge hulls. In Proceedings of the FAST '91, 1st Intl Conf on Fast Sea Transportation, Trondheim, Norway, 17–21 June 1991; Tapir Publishers: Emmen, The Netherlands, 1991; p. 125. Available online: https://trid.trb.org/View/439784 (accessed on 12 January 2025).
31. Lakatos, M.; Sahk, T.; Kaarma, R.; Tabri, K.; Kõrgesaar, M.; Andreasson, H. Experimental testing of spray rails for the resistance reduction of planing crafts. In *Trends in the Analysis and Design of Marine Structures - Proceedings of the 7th International Conference on Marine Structures, MARSTRUCT 2019, Dubrovnik, Croatia, 6–8 May 2019*; CRC Press: Boca Raton, FL, USA, 2019.
32. Ferziger, J.H.; Perić, M.; Street, R.L. *Computational Methods for Fluid Dynamics*; Springer: Berlin/Heidelberg, Germany, 2019.
33. Reynolds, O. IV. On the dynamical theory of incompressible viscous fluids and the determination of the criterion. *Philos. Trans. R. Soc. Lond. A* **1895**, *186*, 123–164. [CrossRef]
34. *ITTC 7.5-03-02-03*; Recommended Procedures and Guidelines: Practical Guidelines for Ship CFD. International Towing Tank Conference: Zürich, Switzerland, 2021.
35. De Luca, F.; Mancini, S.; Miranda, S.; Pensa, C. An Extended Verification and Validation Study of CFD Simulations for Planing Hulls. *J. Ship Res.* **2016**, *60*, 101–118. [CrossRef]
36. Viola, I.M.; Flay, R.G.J.; Ponzini, R. CFD analysis of the hydrodynamic performance of two candidate America's Cup AC33 hulls. *Trans. R. Inst. Nav. Archit. Part B Int. J. Small Craft Technol.* **2012**, *154*, B1–B12. [CrossRef]
37. *ITTC 75-03-01-01 Rev 04*; Uncertainty Analysis in CFD Verification and Validation, Methodology and Procedures. International Towing Tank Conference: Zürich, Switzerland, 2021.
38. Eça, L.; Hoekstra, M. A procedure for the estimation of the numerical uncertainty of CFD calculations based on grid refinement studies. *J. Comput. Phys.* **2014**, *262*, 104–130. [CrossRef]
39. Eca, L.; Hoekstra, M. Discretization Uncertainty Estimation based on a Least Squares version of the Grid Convergence Index. In Proceedings of the Second Workshop on CFD Uncertainty Analysis, Lisbon, Portugal, 1 October 2006; Instituto Superior Tecnico: Lisbon, Portugal, 2006; pp. 1–27.
40. Sulman, M.; Mancini, S.; Niazmand Bilandi, R. Numerical Investigation of Single and Double Steps in Planing Hulls. *J. Mar. Sci. Eng.* **2024**, *12*, 614. [CrossRef]